BIOCHEMISTRY
including biophysical chemistry & molecular biology

Article

pubs.acs.org/biochemistry

Characterization of Early Stage Intermediates in the Nucleation Phase of Aβ Aggregation

Jiali Zhai,[†,§] Tzong-Hsien Lee,[†,§] David H. Small,[‡] and Marie-Isabel Aguilar*[,†]

[†]Department of Biochemistry and Molecular Biology, Monash University, Clayton, Victoria 3800, Australia
[‡]Menzies Research Institute Tasmania, University of Tasmania, Hobart, Tasmania 7000, Australia

ABSTRACT: Alzheimer's disease (AD) is a common form of dementia, which is characterized by the presence of extracellular amyloid plaques comprising the amyloid β peptide (Aβ). Although the mechanism underlying AD pathogenesis remains elusive, accumulating evidence suggests that the process of amyloid fibril formation is a surface-mediated event, which plays an important role in AD onset and progression. In this study, the mechanism of Aβ aggregation on hydrophobic surfaces was investigated with dual polarization interferometry (DPI), which provides real-time information on early stages of the aggregation process. Aggregation was monitored on a hydrophobic C18 surface and a polar silicon oxynitride surface. The DPI results showed a characteristic Aβ aggregation pattern involving a decrease in the density of Aβ at the surface followed by an increase in the thickness on the hydrophobic C18 chip. Most importantly, the DPI measurements provided unique information on the early stages of Aβ aggregation, which is characterized by the presence of initially slow nucleus formation process followed by exponential fibril elongation. The dimensions of the putative nucleus corresponded to a thickness of ∼5 nm for both Aβ40 and Aβ42, which may represent about 10−15 molecules. The results thus support the nucleation-dependent polymerization model as indicated by the presence of a nucleation phase followed by an exponential growth phase. These results are the first reported measurements of the real-time changes in Aβ molecular structure during the early stages of amyloid formation at the nanometer level.

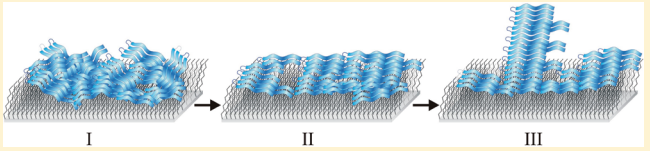

Alzheimer's disease (AD) is a progressive neurodegenerative disease, characterized pathologically by extracellular amyloid plaques that are formed as a result of amyloid β peptide (Aβ) accumulation in the brain.[1−3] Although the mechanism underlying AD pathogenesis remains elusive, a growing body of evidence suggests that Aβ aggregation and deposition into fibrils is causally linked with AD.[1−3] According to the widely accepted amyloid cascade hypothesis, an increase in production of soluble nontoxic Aβ results in accumulation of Aβ, which subsequently undergoes conformational change and self-assembly into insoluble fibrils. While the identity of the toxic form of Aβ is unknown, the accumulation of Aβ aggregates triggers a cascade of pathological events, leading to widespread neuronal dysfunction and eventually dementia and death.[2] It is now generally accepted that soluble Aβ oligomers, rather than the mature fibrils, are the major toxic species since there is poor correlation between the number of amyloid plaques in the brain and the degree of cognitive decline of AD patients.[4−8] However, while the factors that influence Aβ assembly and the neurotoxic action of Aβ aggregates remain poorly understood, several studies have implicated the cell membrane in the aggregation of Aβ.[9−12] In particular, Aβ aggregation can be strongly influenced by a complex interplay between hydrophobic and electrostatic forces. However, the complex properties of the membrane bilayer make it difficult to characterize the nature of the early stage intermediates. In order to dissect the relative contribution of these surface phenomena on Aβ aggregation pathways, chemically modified surfaces with well-defined physical properties can be used as model systems to mimic specific interaction forces.[13−15]

To fully understand amyloid fibril formation and the neurotoxicity of Aβ aggregates, the structures and properties of Aβ monomers, intermediate aggregates and fibrils, and the on-pathway intermediates need to be defined. Aβ is a ∼4 kDa peptide containing 40−42 amino acid residues that is generated from proteolytic cleavage of a much larger transmembrane amyloid precursor protein (APP) by β- and γ-secretases. Cleavage of APP can give rise to two forms of Aβ with different lengths depending on the cleavage site. Aβ40 and Aβ42 with 40- or 42-amino acid residues, respectively, are the two major species. Soluble Aβ is a monomeric peptide and adopts a mainly random coil or α-helical structure upon release.[16] Numerous structural studies have shown that Aβ is primarily α-helical in organic solvents while in aqueous physiological buffers it predominantly forms β-sheet.[16] The α−β conformational change is thought to be initiated by the hydrophilic N-terminus, while the C-terminus which is a hydrophobic region, has a higher propensity for β-sheet structure and mediates β-sheet aggregation.[16] Amyloid fibril formation involves the formation of a range of molecular weight species. Aβ oligomers are reported to be soluble, globular aggregates about 5 nm in diameter, consisting of 2−5 monomers.[4,17] Protofibrils are

Received: December 18, 2011
Revised: January 15, 2012
Published: January 24, 2012

linear aggregates that are 4−11 nm in diameter and 20−200 nm in length according to transmission electron microscopy (TEM) studies.[7,18,19] X-ray diffraction techniques revealed that the mature fibril, 7−12 nm in diameter, consists of three to six laterally associated filaments and a characteristic cross-β-sheet structure. The cross-β-sheet structure comprises an array of β-sheets propagating into a helical-twisted fibril with the β-strand perpendicular to the long axis of the fibril.[16,20]

The formation of amyloid fibrils is a complex process, which starts from proteolytic processing of APP to generate Aβ and ends with the formation of mature amyloid fibrils by Aβ aggregation, involving a variety of intermediates. However, the mechanism underlying amyloid fibril formation is still poorly understood. Based on in vitro studies of Aβ aggregation, two kinetic models have been proposed to quantitatively describe the assembly procedure. These include the nucleation-dependent polymerization model which postulates that amyloid fibril formation initiates from the assembly of monomers into a "nucleus", the process of which is both thermodynamically and kinetically unfavorable and is followed by elongation steps via irreversible addition of monomers.[21] Hence, there is a lag phase corresponding to the rate-limiting nucleus formation step. Once the nucleus is formed, it acts as a seed for exponential fibril growth. The second model is referred to as the template assembly model, wherein fibril elongation occurs via reversible addition of a soluble monomer to a pre-existing fibril, followed by a conformational change to an aggregation-competent state and hence the irreversible association onto the end of the fibril.[22−24] Esler et al.[23] suggested a template-dependent dock-lock mechanism for the explanation of their kinetic data on the association/dissociation rate of radiolabeled Aβ monomers onto synthetic Aβ fibrils. In the "dock" phase, the deposition of Aβ monomers onto synthetic Aβ fibrils, which acts as a template, was readily reversible. Once the equilibrium of this reversible association was established, the rate-limiting conversion from aggregation-incompetent state to aggregation-competent state in the "dock" phase occurred in a time-dependent manner. After the structural transition, the added Aβ, now in the aggregation-competent state, irreversibly associated onto the end of the amyloid fibril and provided a new binding site for the second Aβ monomer.[23]

Despite these extensive studies, there is still a significant lack of structural information about the nature of early stage Aβ intermediates, particularly during the adsorption to biological or chemical surfaces. We have previously analyzed the aggregation of Aβ by high-resolution microscopy and documented the structures of an Aβ monomer, dimer, tetramer, and oligomers by high-resolution scanning tunneling microscopy (STM).[17] We also investigated the surface-mediated aggregation of Aβ by atomic force microscopy and demonstrated the influence of different surface structures on the aggregation process.[13] However, the structure of the early stage intermediates and the various factors that influence Aβ assembly and fibril formation are still far from understood.

The overall aim of this study was to investigate the binding of Aβ onto different surfaces and the subsequent aggregation and fibril formation process in real time. Optical techniques have played an important role in the study of the mechanisms and kinetics of Aβ aggregation, with instruments utilizing for example, surface plasmon resonance spectroscopy (SPR), to monitor molecular events occurring within the first few hundred nanometers of a sensor surface.[25] However, limited information on the molecular orientation of molecules at the surface is obtained with commercially available SPR instruments. By comparison, dual polarization interferometry (DPI) is an optical biosensing technique that analyzes thin layers adsorbed to planar surfaces within aqueous environments and allows the simultaneous measurement of both the thickness and the density of adsorbed protein monolayers in real time.[26−31] In this study, we have measured the real-time changes in mass, thickness, and density using DPI to monitor the formation of early stage intermediates following adsorption of Aβ to a chemically defined polar and a hydrophobic surface. The results demonstrate previously undetectable changes in the molecular orientation of Aβ molecules at surfaces and provide new insight into the early stages of Aβ aggregation.

MATERIALS AND METHODS

Chemicals and Reagents. Recombinant Aβ1−40 and Aβ1−42 (98% purity) were purchased from RPeptides Inc. (Athens, GA). Sodium chloride (NaCl), sodium hydroxide pellets (NaOH), and dimethyl sulfoxide (DMSO) were obtained from BDH (Kilsyth, Australia). 4-(2-Hydroxyethyl)-1-piperazineethanesulfonic acid (HEPES) and 3[(3-cholamidopropyl)dimethylammonio]propanesulfonic acid (Chaps) were purchased from Sigma (St. Louis, MO). Analytical grade methanol and chloroform were purchased from Merck (Kilsyth, Australia), and ethanol was obtained from Ajax (Sydney, Australia). Water was quartz distilled and deionized in a Milli-Q system (Millipore, Bedford, MA). HPLC grade water was purchased from Merck (Darmstadt, Germany).

Peptide Sample Preparation. The purity and accurate molecular mass of both peptides were checked by C18 reversed phase HPLC coupled with ESI ion trap mass spectrometry. The organic solvent DMSO has been used for solubilization of preformed aggregates and has been reported to render monomeric Aβ in an α-helical conformation.[16,32] Peptides were dissolved in DMSO at a concentration of 2 mM, aliquoted, snap frozen in liquid N_2, and stored at −80 °C until use. Just before the experiment, aliquots of the peptide stock solutions were diluted in HEPES buffer (20 mM HEPES, 150 mM NaCl, pH 7.4) to 5 and 10 μM. The HEPES buffer was filtered through a 0.45 μm syringe filter and degassed prior to use.

DPI Analysis of Aβ Aggregation. *DPI Optical Technology.* DPI is a recently developed optical sensing waveguide technique which allows the simultaneous measurement of thickness and density of a molecule layer on a sensor surface in real time.[30,33,34] The basic optical principle underpinning the technique is described elsewhere.[33,34] DPI technology exploits two polarization modes, the transverse magnetic (TM) and transverse electric (TE) polarization modes traveling through a dual-slab waveguide, which consists of an upper sensing waveguide and a lower reference waveguide. Laser light travels along both the sensing and reference waveguide generating interference fringe patterns at the exit. Such interference fringes are recorded at the far field. As molecules adsorbed onto the sensing waveguide, the binding event influences the evanescent wave of the sensing waveguide and hence changes the phases of interference fringe patterns. The phase responses for both TM and TE are measured during a binding event and were used to derive the absolute values of thickness and RI by solving Maxwell's equation of electromagnetic radiation.[30] A unique combination of thickness and RI values for the layer condition was obtained at each time point.

DPI Instrumentation. Aβ−surface interactions were studied using an AnaLight 200 coupled with FB80 unmodified hydrophilic silicon oxynitride chip or hydrophobic C18-functionalized chip (Farfield Group, UK). Each of the Aβ−surface interactions was replicated parallel in two channels. Before each experiment, the chip surface was cleaned *ex situ* with Hellmanex II and isopropanol for unmodified chip and C18 chip, respectively. Each chip was rinsed with methanol and HPLC water. The desired volume of analyte was injected over the sensor chip using a six-port Rheodyne injector valve on both of the two sensing channels.

The calibration and linearization procedures are essential steps to characterize the sensor chip substructure and the bulk RI of the running buffer in DPI measurements. The chip calibration is used to define the boundary position between the chip surface and the bulk solution, referred to as the solid−liquid surface. The chip was calibrated at 20 °C by injecting 80% ethanol/water (w/w) at a flow rate of 50 μL/min for 2 min. The HEPES bulk buffer solution was calibrated at 20 and 37 °C against HPLC water (50 μL/min for 2 min). A linearization procedure removes the periodic errors from the defects of the fringe images in the phase measurement and was performed by allowing the 80% ethanol to buffer transition step to take place. After the calibration and linearization procedure, HEPES buffer flow was continued until a stable baseline was achieved.

Measurements of Aβ Aggregation. The sample loop and injection needle were thoroughly rinsed with a minimum of 6 mL of HEPES buffer. Freshly prepared Aβ40 and Aβ42 solution (10 and 5 μM, respectively) were then injected over the chip surface at 25 μL/min for 7 min. The HEPES buffer flow was stopped when the peptide solution covered the chip lipid surface and the Aβ peptides were incubated on the surface and the changes in the RI and thickness were monitored for a period of 48 h at 37 °C. The bulk buffer was corrected with a blank injection of HEPES/DMSO buffer. Peptide was injected over two flow cells to give one set of replicates, and each experiment was repeated at least once to give four replicates overall.

Data Processing and Analysis. The recorded TM and TE phase changes were processed using Analight Software Version 2.0. Based on the RI values of 80% ethanol (1.3590) and HPLC water (1.3309), the waveguide layer parameters and the bulk RI can be characterized. The bare surface was set as the experimental zero point for subsequent layers that formed on the surface and extended out into the bulk solution when analytes were added to the sensing channels. The bulk RI of HEPES buffer was determined as 1.3374 and was used to correct the resolved layer geometric parameters of each Aβ binding experiment. The resulting resolved RI and thickness were used to calculate the layer density and mass of Aβ on each surface according to the following equations:

$$\text{layer density (g/cm}^3\text{)} = \frac{D_a(\text{RI} - \text{RI}_b)}{\text{RI}_a - \text{RI}_b}$$

$$\text{mass (ng/mm}^2\text{)} = \text{layer density (g/cm}^3\text{)} \times \text{thickness (nm)}$$

where D_a is the density of analyte (0.71 g/cm^3 for proteins), RI_a is the RI of analyte (1.465 for proteins), RI_b is the bulk RI, and RI is the real time absolute refractive index value of a layer.

The surface coverage of the peptide deposition was also determined by the equation

$$\text{surface coverage (\%)} = \frac{\text{layer density} \times 100}{\text{density protein}}$$

Each data set was processed individually, and calculated parameter values were within a 10% range of the average.

RESULTS

Many studies on amyloid fibril formation have shown that the *in situ* aggregation of Aβ depends on the physicochemical nature of the model surfaces.[18,19,35−37] DPI was therefore used to obtain new detailed information on Aβ−surface interactions by measuring both the thickness and the density changes in real time. To study the effect of the surface properties on the Aβ aggregation process, the aggregation of Aβ was studied on two different chip surfaces. Freshly prepared solutions of either Aβ40 and Aβ42 were injected over a hydrophilic silicon oxynitride chip or a hydrophobic C18-coated chip, and the subsequent aggregation event was monitored in real time for a period of 48 h at 37 °C. The C18 chip provides a strong hydrophobic surface that may exert significant effects on the structural properties of the adsorbed peptide layer. At the end of the peptide injection, peptide solution covered the chip surface, and the HEPES buffer flow was stopped. The subsequent aggregation process was monitored in real time at 37 °C for a period of 48 h. Since the DMSO in the sample has a large RI and generates a large bulk effect, a DMSO/HEPES buffer blank was injected over the chip surface. Although there was an increase in the raw TM and TE responses, the resolved layer properties obtained from the TM and TE values did not show significant changes (data not shown).

Initial Binding of Aβ40 to Silicon Oxynitride and C18 Surfaces. Figure 1 shows the change in the refractive index, mass, and thickness over the first 25 min of deposition and incubation of Aβ40 monomers following deposition onto the unmodified silicon oxynitride chip at a concentration of (A) 10 μM or onto the C18 chip at (B) 5 μM or (C) 10 μM. The thickness and refractive index values are derived from the raw TM and TE values, and the refractive index is used to determine the mass values. The peptide solution was injected for 7 min, during which time an increase in binding was observed followed by equilibration. The values of thickness, density, and mass deposited for Aβ40 3 min after the end of injection were measured. Table 1 thus summarizes the structural properties for each Aβ layer 10 min after the beginning of each injection and deposition onto the chip surface.

Aβ40 formed a peptide layer on the silicon chip with a thickness of 0.52 nm and mass of 0.73 ng/mm^2. In comparison, on the C18 chip at 5 μM, Aβ40 formed a 1.09 nm thick layer with a mass of 1.36 ng/mm^2 as shown in Figure 1B. This experimental thickness is twice the thickness observed on the unmodified silicon chip and is in good agreement with the dimensions of Aβ layers on mica or graphite surfaces, which have similar surface properties to the unmodified and C18 chip used in the present study.[13,17−19,35−38] In particular, we and others have demonstrated by AFM that Aβ40 and Aβ42 oligomers or small aggregates form on different substrates with a peptide layer corresponding to 1−5 nm in height.[13,17−19,35−38]

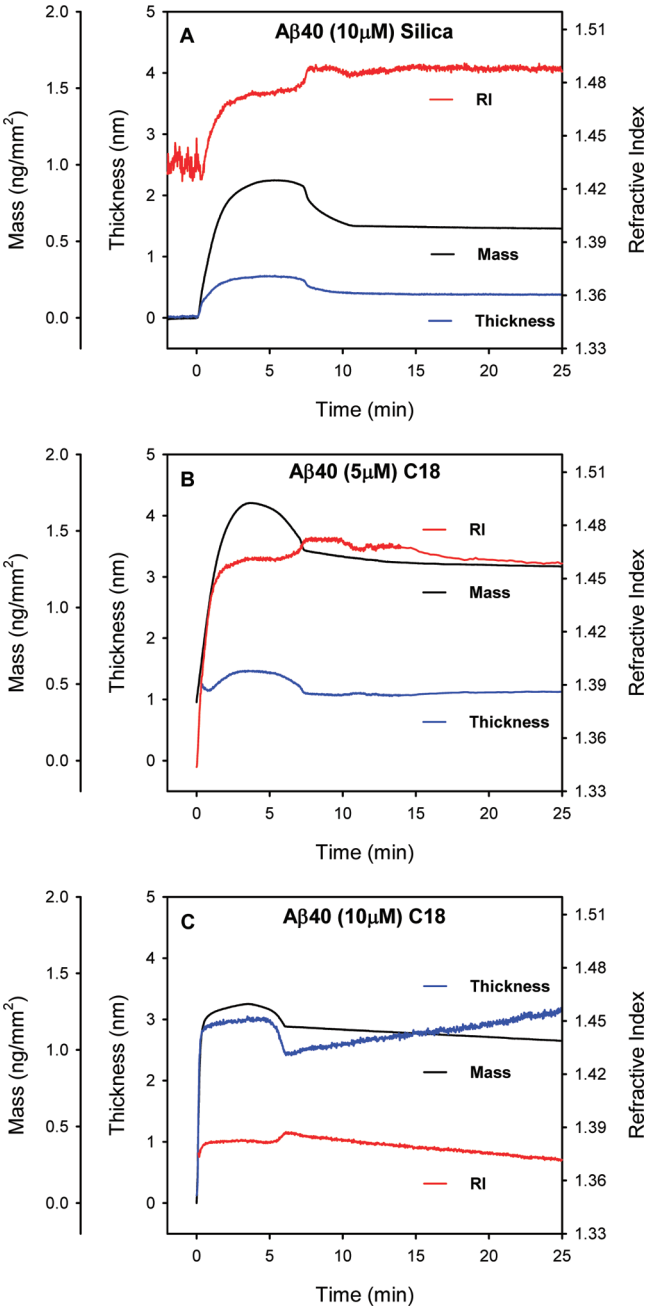

Figure 1. Real-time monitoring for the first 25 min of Aβ40 aggregation process on the (A) unmodified silicon oxynitride chip at 5 μM, (B) the C18 chip at 5 μM, or (C) the C18 chip at 10 μM. Freshly prepared monomeric Aβ40 was injected over each chip at 25 μL/min for 180 s. The analysis temperature was 37 °C.

At 10 μM (Figure 1C), Aβ40 formed a 2.40 nm thick layer on the C18 chip with a mass of 1.17 ng/mm^2. Thus, a similar mass of Aβ40 adsorbed at the higher concentration, but the peptide layer exhibited double the thickness observed for 5 μM Aβ40. In addition, the mass and thickness values did not reach a steady value as was apparent at 5 μM on the C18 chip or on the silicon chip at 10 μM. These constantly changing parameters are likely to reflect the initial stages of aggregation as discussed in detail below.

Initial Binding of Aβ42 to Silicon Oxynitride and C18 Surfaces. Figure 2 shows the corresponding changes in the refractive index, mass, and thickness over the first 25 min of

Table 1. Summary of Values of Thickness, Density, and Mass Deposited for Aβ40 and Aβ42 Aggregation on the Unmodified and C18 Chip Surfaces at the End of the Peptide Injection[a]

peptide	chip	concn (μM)	mass (ng/mm^2)	thickness (nm)	density (g/cm^3)
Aβ40	silica	5	0.73	0.52	1.38
	C18	5	1.36	1.09	1.24
	C18	10	1.17	2.40	0.49
Aβ42	silica	5	1.51	2.33	0.72
	C18	5	1.46	2.12	0.72

[a]The values were obtained from the resolved sensorgrams of Aβ peptide layers on bare chips. The response was allowed to stabilize for 5 min after the peptide injection, and the corresponding values of the surface properties were recorded.

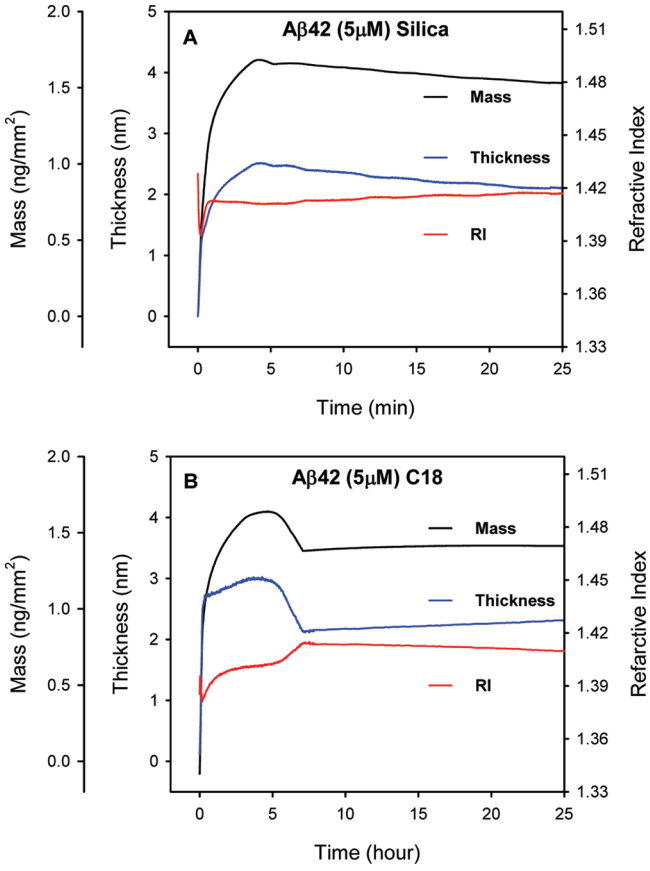

Figure 2. Real-time monitoring for the first 25 min of Aβ42 aggregation process on the (A) unmodified silicon oxynitride chip at 5 μM or (B) the C18 chip at 5 μM. Freshly prepared Aβ42 was injected over each chip at 25 μL/min for 180 s. The analysis temperature was 37 °C.

deposition and incubation of Aβ42 following deposition onto (A) the unmodified silicon oxynitride chip or (B) the C18 chip at a concentration of 5 μM. Since Aβ42 aggregates more rapidly than Aβ40,[39] a concentration of 5 μM Aβ42 was used to study the aggregation processes on both chip surfaces. As is evident from Figure 2, the Aβ42 layer exhibited similar geometrical properties on both surfaces. On the silicon chip, the thickness was 2.52 nm, which was slightly higher than the thickness of 2.48 nm on the C18 surface. A similar mass of peptide was also deposited on both surfaces with 2.33 and 2.12 ng/mm^2 on the silicon and C18 chip, respectively. Thus, at the initial binding

dx.doi.org/10.1021/bi201871r | Biochemistry 2012, 51, 1070–1078

stages, while there was a significant difference in the layer properties for Aβ40 in each surface with more mass and higher thickness on the C18 chip, Aβ42 deposited with a similar mass and thickness on both surfaces.

Surface-Mediated Aggregation of Aβ40 and Aβ42. Following deposition, each peptide was incubated on the surface and the system was monitored for 48 h. In addition to mass and surface thickness, the density of the adsorbed layer was also measured. Figure 3 shows the changes in (A) mass, (B) thickness, and (C) density over the first 10 h for both Aβ40 and Aβ42 on each surface. As can be seen from Figure 3A, the mass remained constant over the entire incubation time on the bare silicon oxynitride chip for both Aβ40 and Aβ42. Figure 3B,C also shows that there was no significant change in the thickness or the density of the peptide layer over this time period at 37 °C on the unmodified silicon oxynitride chip. No change in the mass, thickness, or density was also observed for the entire 48 h incubation time (data not shown).

In contrast, incubation of both Aβ40 and Aβ42 on the C18 chip resulted in a large mass increase as shown in Figure 3A. Inspection of Figure 3B reveals that these increases in mass also coincided with sharp increases in the thickness of the layer. The time at which these increases in physical properties were observed varied with each sample and are summarized in Table 2. The mass increases occurred at 8.5 and 1.2 h of incubation for Aβ40 at 5 and 10 μM, respectively, demonstrating a concentration-dependent process. For Aβ42 the mass increase occurred after 5.8 h at 5 μM. In addition, the thickness changes were observed just prior to the mass increases, occurring at 7.5 and 1.0 h for Aβ40 and 5 h for Aβ42. Since the DPI system has a detection limit of 100 nm above the sensor surface, thickness values greater than 100 nm are outside the measurement range.

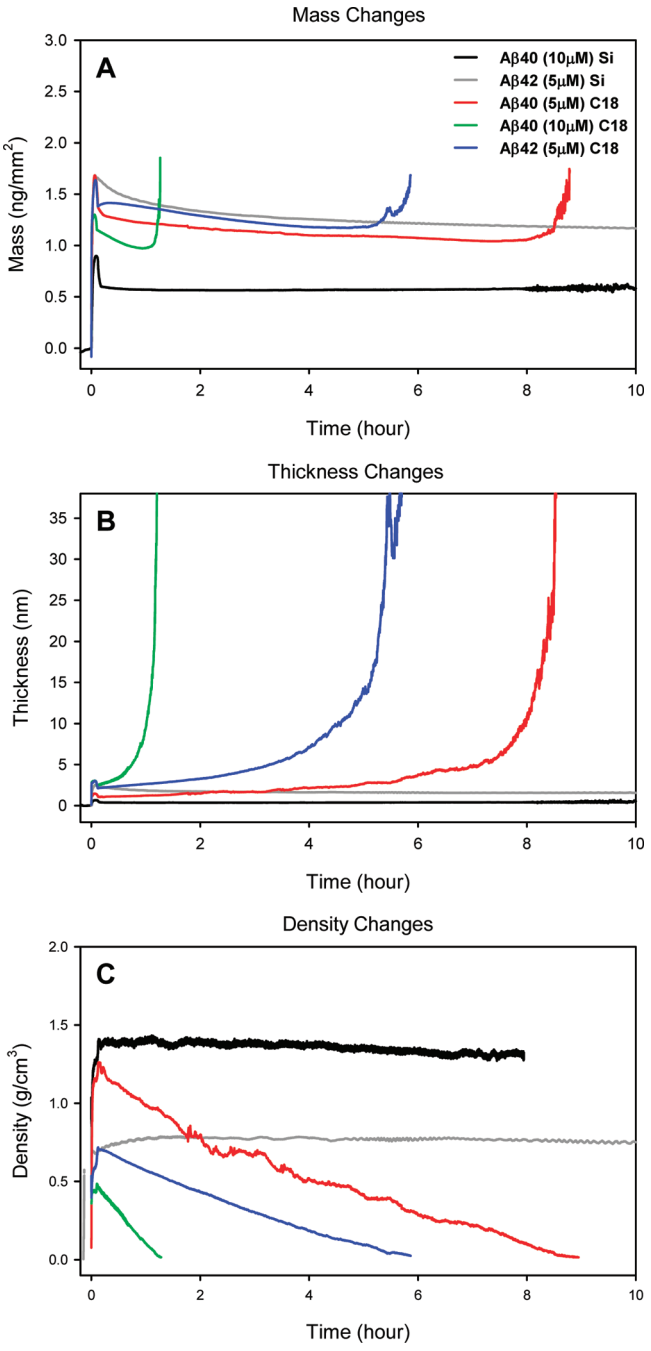

Figure 3. Overlay of the real-time changes in (A) mass, (B) thickness, and (C) density of the adsorbed peptide layer for either Aβ40 or Aβ42 aggregation on the unmodified silicon oxynitride chip or the C18 chip over 10 h. The mass data in (A) are truncated at 1.5−1.7 mass units as the raw TM and TE values cannot be resolved at the thickness values greater than 100 nm.

Table 2. Summary of the Time at Which Rapid Fibril Formation Was Observed for Aβ40 and Aβ42 Aggregation on the Unmodified Silicon Oxynitride and C18 Chip Surfaces

peptide	chip	concn (μM)	time of mass increase (h)	time of thickness increase (h)	rate of density decrease (g/(cm^3 h))
Aβ40	silica	5			
	C18	5	8.5	7.5	0.16
	C18	10	1.2	1.0	0.38
Aβ42	silica	5			
	C18	5	5.8	5	0.14

Analysis of the corresponding density changes during the incubation on the C18 chip (Figure 3C) revealed that the density of the peptide layer decreased immediately upon injection, prior to any notable changes in either thickness or mass. The rate of this decrease was faster at the higher concentration of Aβ40 with a linear rate of 0.16 and 0.38 g/(cm^3 h) at 5 and 10 μM, respectively. Overall, this increase in the rate of change in layer properties at higher concentrations further demonstrates that this phenomenon is a concentration-dependent process. By comparison, the density change for 5 μM Aβ42 of 0.14 g/(cm^3 h) was similar to 5 μM Aβ40.

DISCUSSION

Aβ aggregation is an important step in the pathogenesis of Alzheimer's disease, and there is increasing evidence that lower molecular weight oligomeric forms of Aβ may be the more toxic species in vivo. However, the various factors that influence Aβ assembly are still far from understood. The overall aim of this study was to investigate the binding of Aβ onto different surfaces and the subsequent aggregation and fibril formation process in real time utilizing DPI and obtain new insight into the early stages of Aβ aggregation. In particular, the real-time changes in mass, thickness, and density provide a new approach to studying Aβ aggregation.

dx.doi.org/10.1021/bi201871r | Biochemistry 2012, 51, 1070−1078

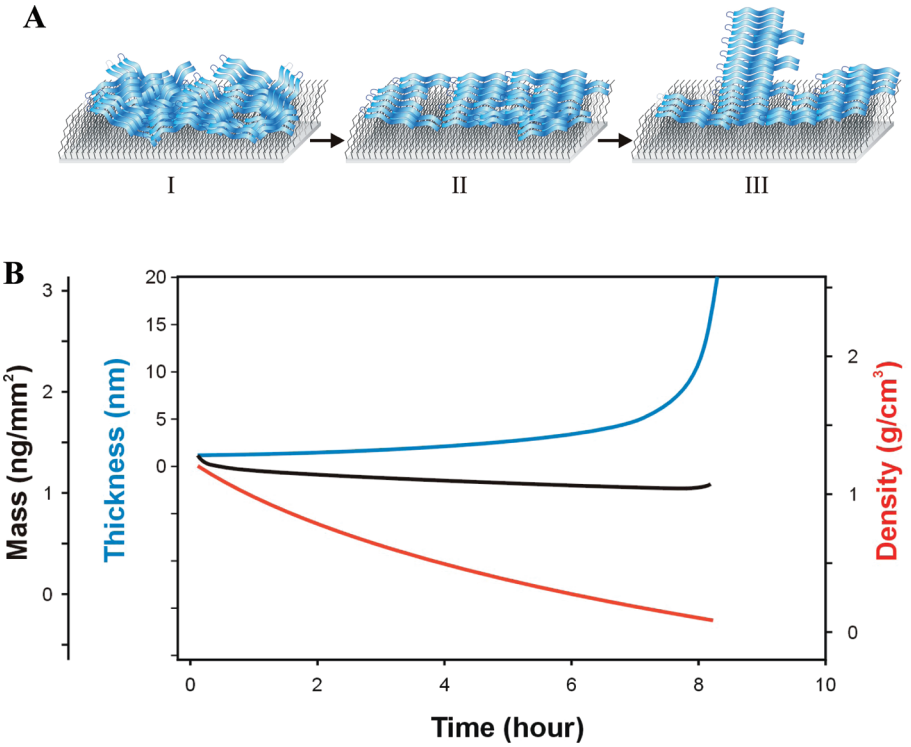

Figure 4. Schematic representation of the proposed model for real-time measurement of Aβ aggregation on the C18 chip by DPI. (A-I) On the C18 chip surface, the observed mass corresponds to peptide molecules bound directly to the surface in a range of different orientations presumably with different affinity. During the incubation period, some bound molecules of Aβ dissociate and rebind to the surface in an amyloidogenic orientation, causing a continual decrease in layer density and results in the formation of the critical amyloidogenic nucleus (A-II). As the critical point is reached, the protofibrils or fibrils which are also likely to be forming in solution quickly associate with the Aβ nucleus on the chip surface, causing a rapid growth in thickness and mass (A-III). (B) The characteristic profile of density, thickness, and mass changes with distinct kinetic phases which supports the nucleation-dependent polymerization model for Aβ40 and Aβ42 aggregation on the C18 chip.

The adsorption of Aβ40 and Aβ42 to the unmodified silicon oxynitride chip revealed no changes in the mass bound, the layer thickness, or the density over 24−48 h. While mass increases have been previously observed on the unmodified silicon chip at a much higher concentration of 50 μM Aβ40,[40] Aβ40 is likely to form oligomers in solution at this higher concentration which upon binding to the chip is likely to readily promote aggregation. We[13,17] and others[38,41] have previously analyzed the aggregation of Aβ by high resolution microscopy and reported the structures of an Aβ monomer, dimer, tetramer, and oligomers by high-resolution STM. Analysis of the monomeric species revealed that Aβ40 adopts a β-sheet structure with molecular height measurements of ~0.6 nm.[17] The dimensions of the Aβ40 layer in this study of 0.5 nm thickness therefore suggest that the initial layer is likely to represent monomers of Aβ40 deposited onto the surface in a β-sheet conformation. By comparison, the thickness of the Aβ42 layer on the silicon chip was 2.33 nm, which suggests that Aβ42 deposited as dimers or that monomers bound in a conformation that folds back via a hairpin similar to that previously suggested by a number of studies.[42] Irrespective of the precise conformation of both Aβ40 and Aβ42, neither molecule exhibited any change in layer properties on the bare chip, suggesting that the orientation of the bound Aβ on the unmodified chip prevented the binding of subsequent molecules to either exposed chip surface or adsorbed Aβ molecules and that the adsorbed conformation is non-amyloidogenic.

In contrast, there were dramatic changes in mass, thickness, and density for both Aβ40 and Aβ42 on the C18 chip. While these properties remained relatively constant over 48 h on the unmodified silicon oxynitride chip, there was a steady decrease in density throughout the incubation period from the time of injection and a sharp increase in thickness and mass after a critical point on the hydrophobic C18 surface. This behavior is consistent with a nucleation-dependent polymerization model in which the initial nucleation phase corresponds to the steady decrease in the layer density and a small change in the thickness. When the critical point was reached, the combination of an exponential increase in thickness and mass is likely to correspond to the fast protofibril or fibril elongation phase. Total internal reflection fluorescence microscopy has been used by others to study Aβ40 aggregation on a range of surfaces including C18 surfaces and demonstrated that surface properties strongly influence the morphology of the Aβ40 aggregates.[19] The results of the present study also indicate that the orientation of Aβ40 and Aβ42 on the C18 chip is different to that on the unmodified chip and facilitates the subsequent aggregation and fibril formation at these low concentrations.

The most significant aspect of these results is the first reported measurement of the real time changes in molecular structure of the early stages of amyloid formation at the nanometer level in terms of the density and thickness of the layer. While it is well accepted that the early stages of fibril formation involve stepwise addition of monomers to generate a nucleus from which the exponential fibril growth ensues, it has

dx.doi.org/10.1021/bi201871r | *Biochemistry* 2012, 51, 1070−1078

been difficult to obtain experimental data to confirm this at molecular resolution. Close analysis of the layer dimensions at the early stage of incubation reveals a significant density change from the outset. When the density decreases with little or no change in mass, the most likely explanation is the formation of linear aggregates growing away from the surface as the weakly associated Aβ40 molecules rearrange to dock onto a prebound Aβ40 molecule. Thus, there is a slow growth of the nucleus which corresponds to a thickness of ~5 nm for both Aβ40 and Aβ42, which in turn may represent about 10−15 molecules.

Based on the structural and orientational changes in Aβ during incubation on the C18 chip, a schematic model of the real-time surface-mediated events of Aβ aggregation is proposed and shown in Figure 4. The Aβ40 and Aβ42 aggregation experiments on the C18 chip showed a characteristic profile of density and thickness changes with distinct kinetic phases which supports the nucleation-dependent polymerization model (Figure 4B). The nucleation phase corresponded to the initial incubation period, whereby the density of the layer decreased linearly. This pattern was also faster at higher concentrations and also more rapid for Aβ42, reflecting the higher aggregation propensity of Aβ42. When the nucleus was formed and the critical point was reached, the thickness and mass increased sharply, which corresponded to the rapid elongation phase of protofibrils or fibrils. In terms of the molecular events at the surface, the orientation of the deposited Aβ monomers or oligomers on the unmodified chip surface is such that the outward face of each molecule does not allow binding of subsequent molecules at low concentrations. However, on the hydrophobic C18 surface, the observed mass corresponds to peptide molecules bound directly to the surface in a range of different orientations presumably with different affinity (Figure 4A-I). The initial binding of Aβ to the surface is therefore kinetically driven to give a "kinetic" orientation. However, upon incubation, Aβ can reorient to a more thermodynamically stable orientation, which leads to a decrease in density. Therefore, during the incubation period, some bound molecules of Aβ dissociate and rebind to the surface in an amyloidogenic orientation, causing a continual decrease in layer density and results in the formation of the critical amyloidogenic nucleus (Figure 4A-II). As the critical point is reached, the protofibrils or fibrils which are also likely to be forming in solution quickly associate with the Aβ nucleus on the chip surface, causing a rapid growth in thickness and mass (Figure 4A-III). The time required for the formation of the critical nucleus on the chip surface depends on the concentration as well as the type of Aβ peptide.

Recent studies using fluorescence correlation spectroscopy (FCS) and transmission electron microscopy have demonstrated the existence of two different pathways of assembly of Aβ.[43] These studies suggested that one pathway leads to the formation of toxic spherical particles of 10−15 nm in diameter while the second pathway leads to fibrils. Moreover, Aβ40 and Aβ42 have been shown to exhibit different molecular recycling properties where the rate of dissociation of Aβ40 monomers from the fibril is much faster than that for Aβ42.[44] Our study suggests that adsorption of Aβ to a specific surface may either enhance aggregation or inhibit or considerably slow down fibril formation by inducing a nonfibrillogenic orientation. It is therefore apparent that surface conditions significantly influence the mechanism of Aβ aggregation which in a cellular context may modulate toxicity depending on the local environment. This conclusion has also been reached by recent studies on the structure and morphology of Aβ40 on different self-assembled monolayers which also demonstrated that Aβ orients differently on different surfaces, which in turn affects the nature of the aggregates formed upon incubation.[14,45,46] Overall, the present study demonstrates the ability of the "in situ" incubation method to give new information on early stage intermediates of Aβ aggregation.

CONCLUSIONS

Real-time measurements of Aβ aggregation upon surface adsorption by DPI demonstrate that the physicochemical properties of the surface influence the orientation of Aβ, which in turn controls the ability of Aβ to undergo aggregation and fibril formation. In particular, a characteristic aggregation pattern for both Aβ40 and Aβ42 was observed with the C18 chip compared to the hydrophilic silicon oxynitride surface. These results confirm that a hydrophobic surface triggers the Aβ aggregation process[14,18,36,37,45,46] and serves as a template for Aβ self-assembly and amyloid fibril formation. Overall, this study provides new insight into the molecular reorganization of Aβ during the nucleation phase which involves significant reorientation of Aβ molecules on the surface. Specifically, this study provides new structural information on the early stages of aggregation and together with other high-resolution techniques such as STM and FCS allows dissection of molecular forces associated with surface-mediated amyloid formation. Moreover, to further explore the mechanism of surface-induced aggregation, DPI has the potential to analyze the efficacy of compounds which interfere with the aggregation process. DPI could also be used to study the interaction of Aβ with model membranes and then correlated with aggregation behavior in the presence of neuronal cell membranes to provide novel insight into the relationship between membrane binding and neurotoxicity. Given that low molecular weight oligomers are more neurotoxic, these results have significance in terms of understanding the mechanism of pathogenesis in AD and protein misfolding in general.

AUTHOR INFORMATION

Corresponding Author

*E-mail: mibel.aguilar@monash.edu; Ph: +61-3-9905-3723; Fax: +61-3-9902-9500.

Author Contributions

[§]These authors contributed equally.

Funding

The financial support of the Australian Research Council, the National Health & Medical Research Council of Australia, and the Potter Foundation is gratefully acknowledged.

Notes

The authors declare no competing financial interest.

ACKNOWLEDGMENTS

The financial support of the Australian Research Council, the National Health & Medical Research Council of Australia, and the Potter Foundation is gratefully acknowledged.

REFERENCES

(1) Gandy, S. (2005) The role of cerebral amyloid-β accumulation in common forms of Alzheimer disease. *J. Clin. Invest. 115*, 1121−1129.

(2) Hardy, J., and Selkoe, D. J. (2002) The amyloid hypothesis of Alzheimer's Disease: progress and problems on the road to therapeutics. *Science 297*, 353−356.

(3) Hardy, J. A., and Higgins, G. A. (1992) Alzheimer's disease: the amyloid cascade hypothesis. *Science 256*, 184−185.
(4) Chromy, B. A., Nowak, R. J., Lambert, M. P., Viola, K. L., Chang, L., Velasco, P. T., Jones, B. W., Fernandez, S. J., Lacor, P. N., Horowitz, P., Finch, C. E., Krafft, G. A., and Klein, W. L. (2003) Self-assembly of Abeta(1−42) into globular neurotoxins. *Biochemistry 42*, 12749−12760.
(5) Demuro, A., Mina, E., Kayed, R., Milton, S. C., Parker, I., and Glabe, C. G. (2005) Calcium Dysregulation and Membrane Disruption as a Ubiquitous Neurotoxic Mechanism of Soluble Amyloid Oligomers. *J. Biol. Chem. 280*, 17294−17300.
(6) Glabe, C. G. (2006) Common mechanisms of amyloid oligomer pathogenesis in degenerative disease. *Neurobiol. Aging 27*, 570−575.
(7) Hartley, D. M., Walsh, D. M., Ye, C. P., Diehl, T., Vasquez, S., Vassilev, P. M., Teplow, D. B., and Selkoe, D. J. (1999) Protofibrillar Intermediates of Amyloid beta -Protein Induce Acute Electrophysiological Changes and Progressive Neurotoxicity in Cortical Neurons. *J. Neurosci. 19*, 8876−8884.
(8) Kayed, R., Sokolov, Y., Edmonds, B., McIntire, T. M., Milton, S. C., Hall, J. E., and Glabe, C. G. (2004) Permeabilization of Lipid Bilayers Is a Common Conformation-dependent Activity of Soluble Amyloid Oligomers in Protein Misfolding Diseases. *J. Biol. Chem. 279*, 46363−46366.
(9) Kakio, A., Nishimoto, S. i., Yanagisawa, K., Kozutsumi, Y., and Matsuzaki, K. (2002) Interactions of Amyloid -Protein with Various Gangliosides in Raft-Like Membranes: Importance of GM1 Ganglioside-Bound Form as an Endogenous Seed for Alzheimer Amyloid. *Biochemistry 41*, 7385−7390.
(10) Subasinghe, S., Unabia, S., Barrow, C. J., Mok, S. S., Aguilar, M. I., and Small, D. H. (2003) Cholesterol is necessary both for the toxic effect of Abeta peptides on vascular smooth muscle cells and for Abeta binding to vascular smooth muscle cell membranes. *J. Neurochem. 84*, 471−479.
(11) Yip, C. M., Darabie, A. A., and McLaurin, J. (2002) Abeta42-peptide assembly on lipid bilayers. *J. Mol. Biol. 318*, 97−107.
(12) Yip, C. M., and McLaurin, J. (2001) Amyloid-beta peptide assembly: a critical step in fibrillogenesis and membrane disruption. *Biophys. J. 80*, 1359−1371.
(13) Losic, D., Martin, L. L., Aguilar, M. I., and Small, D. H. (2006) Beta-amyloid fibril formation is promoted by step edges of highly oriented pyrolytic graphite. *Biopolymers 84*, 519−526.
(14) Wang, Q., Shah, N., Zhao, J., Wang, C., Zhao, C., Liu, L., Li, L., Zhou, F., and Zheng, J. (2011) Structural, morphological, and kinetic studies of beta-amyloid peptide aggregation on self-assembled monolayers. *Phys. Chem. Chem. Phys. 13*, 15200−15210.
(15) Zhao, J., Wang, Q., Liang, G., and Zheng, J. Molecular Dynamics Simulations of Low-Ordered Alzheimer beta-Amyloid Oligomers from Dimer to Hexamer on Self-Assembled Monolayers, *Langmuir*, in press.
(16) Serpell, L. C. (2000) Alzheimer's amyloid fibrils: structure and assembly. *Biochim. Biophys. Acta, Mol. Basis Dis. 1502*, 16−30.
(17) Losic, D., Martin, L. L., Mechler, A., Aguilar, M. I., and Small, D. H. (2006) High resolution scanning tunnelling microscopy of the beta-amyloid protein (Abeta1−40) of Alzheimer's disease suggests a novel mechanism of oligomer assembly. *J. Struct. Biol. 155*, 104−110.
(18) Arimon, M., Diez-Perez, I., Kogan, M. J., Durany, N., Giralt, E., Sanz, F., and Fernandez-Busquets, X. (2005) Fine structure study of Abeta1−42 fibrillogenesis with atomic force microscopy. *FASEB J. 19*, 1344−1346.
(19) Ban, T., Morigaki, K., Yagi, H., Kawasaki, T., Kobayashi, A., Yuba, S., Naiki, H., and Goto, Y. (2006) Real-time and Single Fibril Observation of the Formation of Amyloid beta Spherulitic Structures. *J. Biol. Chem. 281*, 33677−33683.
(20) Sunde, M., Serpell, L. C., Bartlam, M., Fraser, P. E., Pepys, M. B., and Blake, C. C. F. (1997) Common core structure of amyloid fibrils by synchrotron X-ray diffraction. *J. Mol. Biol. 273*, 729−739.
(21) Jarrett, J. T., and Lansbury, P. T. Jr. (1993) Seeding "one-dimensional crystallization" of amyloid: a pathogenic mechanism in Alzheimer's disease and scrapie? *Cell 73*, 1055−1058.
(22) Cannon, M. J., Williams, A. D., Wetzel, R., and Myszka, D. G. (2004) Kinetic analysis of beta-amyloid fibril elongation. *Anal. Biochem. 328*, 67−75.
(23) Esler, W. P., Stimson, E. R., Jennings, J. M., Vinters, H. V., Ghilardi, J. R., Lee, J. P., Mantyh, P. W., and Maggio, J. E. (2000) Alzheimer's Disease Amyloid Propagation by a Template-Dependent Dock-Lock Mechanism. *Biochemistry 39*, 6288−6295.
(24) Hasegawa, K., Ono, K., Yamada, M., and Naiki, H. (2002) Kinetic Modeling and Determination of Reaction Constants of Alzheimer's [beta]-Amyloid Fibril Extension and Dissociation Using Surface Plasmon Resonance. *Biochemistry 41*, 13489−13498.
(25) Aguilar, M. I., and Small, D. H. (2005) Surface plasmon resonance for the analysis of beta-amyloid interactions and fibril formation in Alzheimer's disease research. *Neurotox. Res. 7*, 17−27.
(26) Freeman, N. J., Peel, L. L., Swann, M. J., Cross, G. H., Reeves, A., Brand, S., and Lu, J. R. (2004) Real time, high resolution studies of protein adsorption and structure at the solid-liquid interface using dual polarization interferometry. *J. Phys.: Condens. Matter 16*, S2493−S2496.
(27) Lee, T., Hall, K., Swann, M., Popplewell, J., Unabia, S., Park, Y., Hahm, K., and Aguilar, M. (2010) The membrane insertion of helical antimicrobial peptides from the N-terminus of *Helicobacter pylori* risbosomal protein L1. *Biochim. Biophys. Acta 1798*, 544−557.
(28) Lee, T. H., Heng, C., Swann, M. J., Gehman, J. D., Separovic, F., and Aguilar, M. I. (2010) Real-time quantitative analysis of lipid disordering by aurein 1.2 during membrane adsorption, destabilisation and lysis. *Biochim. Biophys. Acta 1798*, 1977−1986.
(29) Sheu, B. C., Lin, Y. H., Lin, C. C., Lee, A. S., Chang, W. C., Wu, J. H., Tsai, J. C., and Lin, S. (2010) Significance of the pH-induced conformational changes in the structure of C-reactive protein measured by dual polarization interferometry. *Biosens. Bioelectron. 26*, 822−827.
(30) Swann, M. J., Peel, L. L., Carrington, S., and Freeman, N. J. (2004) Dual-polarization interferometry: an analytical technique to measure changes in protein structure in real time, to determine the stoichiometry of binding events, and to differentiate between specific and nonspecific interactions. *Anal. Biochem. 329*, 190−198.
(31) Hirst, D., Lee, T., Unabia, S., Swann, M., Park, Y., Hahm, K., and Aguilar, M. (2011) The effect of acyl chain structure and bilayer phase state on the binding and insertion of HPA3 onto a supported lipid bilayer. *Eur. Biophys. J. 40*, 503−514.
(32) Nilsson, M. R. (2004) Techniques to study amyloid fibril formation in vitro. *Methods 34*, 151−160.
(33) Cross, G. H., Reeves, A. A., Brand, S., Popplewell, J. F., Peel, L. L., Swann, M. J., and Freeman, N. J. (2003) A new quantitative optical biosensor for protein characterisation. *Biosens. Bioelectron. 19*, 383−390.
(34) Cross, G. H., Reeves, A. A., Brand, S., Swann, M. J., Peel, L. L., Freeman, N. J., and Lu, J. R. (2004) The metrics of surface adsorbed small molecules on the Young's fringe dual-slab waveguide interferometer. *J. Phys. D: Appl. Phys. 37*, 74−80.
(35) Blackley, H. K. L., Sanders, G. H. W., Davies, M. C., Roberts, C. J., Tendler, S. J. B., and Wilkinson, M. J. (2000) In-situ atomic force microscopy study of β-amyloid fibrillization. *J. Mol. Biol. 298*, 833−840.
(36) Kowalewski, T., and Holtzman, D. M. (1999) In situ atomic force microscopy study of Alzheimer's beta-amyloid peptide on different substrates: new insights into mechanism of β-sheet formation. *Proc. Natl. Acad. Sci. U. S. A. 96*, 3688−3693.
(37) Wang, Z., Zhou, C., Wang, C., Wan, L., Fang, X., and Bai, C. (2003) AFM and STM study of [beta]-amyloid aggregation on graphite. *Ultramicroscopy 97*, 73−79.
(38) Mastrangelo, I. A., Ahmed, M., Sato, T., Liu, W., Wang, C., Hough, P., and Smith, S. O. (2006) High-resolution Atomic Force Microscopy of Soluble A[beta]42 Oligomers. *J. Mol. Biol. 358*, 106−119.
(39) Klug, G. M., Losic, D., Subasinghe, S. S., Aguilar, M. I., Martin, L. L., and Small, D. H. (2003) Beta-amyloid protein oligomers induced

by metal ions and acid pH are distinct from those generated by slow spontaneous ageing at neutral pH. *Eur. J. Biochem. 270*, 4282−4293.
(40) Farfield. (2007) Measuring early-stage *β*-amyloid aggregation using dual polarisation interferometry, Application Note 004.
(41) Ma, X., Liu, L., Mao, X., Niu, L., Deng, K., Wu, W., Li, Y., Yang, Y., and Wang, C. (2009) Amyloid beta (1−42) folding multiplicity and single-molecule binding behavior studied with STM. *J. Mol. Biol. 388*, 894−901.
(42) Tycko, R. (2006) Molecular structure of amyloid fibrils: insights from solid-state NMR. *Q. Rev. Biophys. 39*, 1−55.
(43) Matsumura, S., Shinoda, K., Yamada, M., Yokojima, S., Inoue, M., Ohnishi, T., Shimada, T., Kikuchi, K., Masui, D., Hashimoto, S., Sato, M., Ito, A., Akioka, M., Takagi, S., Nakamura, Y., Nemoto, K., Hasegawa, Y., Takamoto, H., Inoue, H., Nakamura, S., Nabeshima, Y., Teplow, D. B., Kinjo, M., and Hoshi, M. (2011) Two distinct amyloid beta-protein (Abeta) assembly pathways leading to oligomers and fibrils identified by combined fluorescence correlation spectroscopy, morphology, and toxicity analyses. *J. Biol. Chem. 286*, 11555−11562.
(44) Sanchez, L., Madurga, S., Pukala, T., Vilaseca, M., Lopez-Iglesias, C., Robinson, C. V., Giralt, E., and Carulla, N. (2011) Abeta40 and Abeta42 amyloid fibrils exhibit distinct molecular recycling properties. *J. Am. Chem. Soc. 133*, 6505−6508.
(45) Moores, B., Drolle, E., Attwood, S. J., Simons, J., and Leonenko, Z. (2011) Effect of surfaces on amyloid fibril formation. *PLoS One 6*, e25954.
(46) Zhao, J., Wang, Q., Liang, G., and Zheng, J. (2011) Molecular Dynamics Simulations of Low-Ordered Alzheimer beta-Amyloid Oligomers from Dimer to Hexamer on Self-Assembled Monolayers. *Langmuir 27*, 14876−14887.